nature geoscience

ARTICLES

https://doi.org/10.1038/s41561-019-0384-9

Mobilization of aged and biolabile soil carbon by tropical deforestation

Travis W. Drake[1,2,11*], Kristof Van Oost[3], Matti Barthel[4], Marijn Bauters[5,6], Alison M. Hoyt[7,8], David C. Podgorski[1,2,12], Johan Six[4], Pascal Boeckx[5], Susan E. Trumbore[7,9], Landry Cizungu Ntaboba[10] and Robert G. M. Spencer[1,2]

In the mostly pristine Congo Basin, agricultural land-use change has intensified in recent years. One potential and understudied consequence of this deforestation and conversion to agriculture is the mobilization and loss of organic matter from soils to rivers as dissolved organic matter. Here, we quantify and characterize dissolved organic matter sampled from 19 catchments of varying deforestation extent near Lake Kivu over a two-week period during the wet season. Dissolved organic carbon from deforested, agriculturally dominated catchments was older (^{14}C age: ~1.5 kyr) and more biolabile than from pristine forest catchments. Ultrahigh-resolution mass spectrometry revealed that this aged organic matter from deforested catchments was energy rich and chemodiverse, with higher proportions of nitrogen- and sulfur-containing formulae. Given the molecular composition and biolability, we suggest that organic matter from deforested landscapes is preferentially respired upon disturbance, resulting in elevated in-stream concentrations of carbon dioxide. We estimate that while deforestation reduces the overall flux of dissolved organic carbon by approximately 56%, it does not significantly change the yield of biolabile dissolved organic carbon. Ultimately, the exposure of deeper soil horizons through deforestation and agricultural expansion releases old, previously stable, and biolabile soil organic carbon into the modern carbon cycle via the aquatic pathway.

Tropical soils are major reservoirs of soil organic carbon (SOC) and are estimated to contain approximately one third of the global first-metre SOC stock (~1,325 Pg)[1]. The stability of these vast tropical SOC stocks is threatened by increasing anthropogenic disturbance in the form of deforestation and associated land-use change. A recent global meta-analysis found that the conversion of tropical primary forest to croplands resulted in an average relative SOC loss of 25% (ref. [2]). Given the relevance of these stocks to the global carbon (C) cycle, there is a growing need for fundamental and mechanistic research into how anthropogenic pressures may alter the tropical C cycle.

It is well established that deforestation and land-use change release carbon dioxide (CO_2) via the in situ respiration of SOC in disturbed soils[2–5]. A relatively understudied effect of soil disturbance, however, is the leaching and mobilization of SOC as dissolved organic carbon (DOC)[6]. In northern ecosystems, forest loss and soil disturbance has generally been found to increase DOC losses to streams[7–9], although decreases have also been reported[10,11]. The effect of deforestation on DOC mobilization in tropical ecosystems is not well documented, but recent work in Southeast Asia has shown increases following forest loss, secondary regrowth, and increased freshwater fluxes[12,13]. In addition to changes in DOC concentration and fluxes, the export of aged DOC has been documented in disturbed soils and shown to be positively correlated with human disturbance globally, suggesting that DOC is an important indicator of SOC stability[12,14,15]. Historically, aged DOC sourced from terrestrial ecosystems is assumed to be chemically stable and resistant to biodegradation[16,17]. Recent studies on aged DOC in Arctic aquatic ecosystems and elsewhere, however, suggest that it can be highly biolabile and rapidly oxidized by microbes on release to surface waters, depending on the physicochemical conditions under which it was developed and preserved (that is, in complexes with minerals, permafrost, anoxia, reducing conditions and so on)[18–20]. Little is known about the relationship between DOC biolability and age within tropical ecosystems. Bridging this knowledge gap is important given that the 'lateral' aquatic loss of aged DOC reintroduces aged C into the modern C cycle and is thus analogous to the combustion of fossil fuels, provided the mobilized C is microbially or photo-oxidized to CO_2.

Central Africa's relatively understudied Congo Basin (~3.7 million km^2) represents an ideal tropical forest ecosystem to investigate these processes. The Congo Basin is estimated to contain 20 Pg of SOC in its top metre of soil[21], not including the more than 30 Pg recently mapped and quantified in the inundated swamp forests of the Cuvette Centrale[22]. Currently, the extensive SOC reservoir in the Congo Basin is mostly undisturbed, as the interior lowland forests that protect the soils have remained relatively free from intensive deforestation[23,24]. Deforestation near the basin's eastern and western borders, however, has accelerated due to rapid population growth concurrent with agricultural expansion and charcoal production. For example, the Kivu region of eastern Democratic Republic of Congo (DRC) is estimated to have lost more than 2,400 km^2 of

[1]Department of Earth, Ocean, and Atmospheric Science, Florida State University, Tallahassee, FL, USA. [2]Geochemistry Group, National High Magnetic Field Laboratory, Tallahassee, FL, USA. [3]Earth and Life Institute, Université Catholique de Louvain, Louvain-la-Neuve, Belgium. [4]Department of Environmental Systems Science, ETH Zurich, Zurich, Switzerland. [5]Isotope Bioscience Laboratory, Department of Green Chemistry and Technology, Ghent University, Gent, Belgium. [6]Computational and Applied Vegetation Ecology Lab, Department of Environment, Ghent University, Gent, Belgium. [7]Max Planck Institute for Biogeochemistry, Jena, Germany. [8]Lawrence Berkeley National Laboratory, Berkeley, CA, USA. [9]Earth System Science, University of California, Irvine, CA, USA. [10]Faculty of Agronomy, Université Catholique de Bukavu, Bukavu, Congo. [11]Present address: Department of Environmental Systems Science, ETH Zurich, Zurich, Switzerland. [12]Present address: Pontchartrain Institute for Environmental Sciences, Department of Chemistry, University of New Orleans, New Orleans, LA, USA. *e-mail: draketw@gmail.com

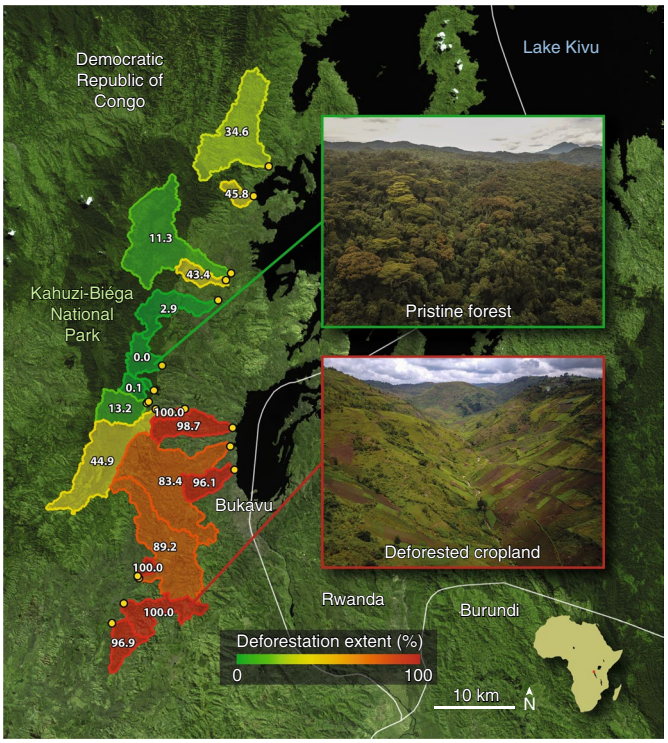

Fig. 1 | Sampling locations and catchment delineations for this study. Sampling locations are yellow points and study catchments ($n = 19$) are coloured from green to red according to their deforestation extent. White numbers overlaying each catchment indicate the areal percentage of deforestation. Inlayed pictures show an aerial view of pristine forest (top) and deforested cropland (bottom). Basemap imagery sourced from Copernicus Sentinel-2 satellite data (2017).

primary forest from 2000 to 2010, approximately 2.7% of the region's forest cover[25].

To assess the impact of deforestation and subsequent conversion to agricultural lands on lateral C losses from tropical soils of the Congo Basin, we measured the concentration, age and biolability of DOC, in addition to the composition of dissolved organic matter (DOM), exported by 19 catchments of varying deforestation extent near Lake Kivu, DRC. Before human settlement and agricultural proliferation in the region, South Kivu was covered by dense tropical forest[26]. Today, the remaining pristine forests in the region are protected within the borders of Kahuzi-Biéga National Park. Our 19 study catchments span 0.7° latitude, range in area from 0.25 to 85.2 km^2 and vary by extent of deforestation from 0.0 to 100.0% (Fig. 1).

Mobilization of aged subsoil C with land-use conversion

Our isotopic results point to land use as a primary control of DOC source and age. The extent of deforestation within a catchment, predominantly a function of agricultural land use, was negatively related to the bulk radiocarbon age of DOC (Fig. 2a and Supplementary Table 1). The DOC from completely deforested catchments had a bulk $\Delta^{14}C$ value of $-179 \pm 16‰$, representing a radiocarbon age of ~1,500 yr BP. These deforested tropical Congo $\Delta^{14}C$-DOC values were slightly more enriched but similar to those measured from other disturbed temperate and Amazonian catchments ($-230‰$ for urban or agricultural watersheds)[14]. In contrast, the pristine catchments draining areas of Kahuzi-Biéga National Park with 100% forest cover displayed a bulk $\Delta^{14}C$-DOC value of $+19.0 \pm 17.9‰$, indicating the export of modern DOC.

Deforestation extent was positively correlated with $\delta^{13}C$-DOC enrichment (Fig. 2b and Supplementary Table 1), with fully deforested and forested values of -22.3 ± 0.4 and $-27.4 \pm 0.5‰$, respectively. A coupled isotopic $\Delta^{14}C$- and $\delta^{13}C$-DOC plot shows how deforestation results in both older and more $\delta^{13}C$-enriched values (coloured points in Fig. 2c). Soil isotopic signatures to 75 cm from the pristine forest of Kahuzi-Biéga National Park revealed a very similar $\Delta^{14}C$- versus $\delta^{13}C$-SOC gradient with depth as DOC with deforestation (black dotted line in Fig. 2c and Supplementary Table 2). Organic carbon from litter and O horizons was modern and relatively depleted in $\delta^{13}C$ ($-28.5‰$), whereas deeper horizons became older and more enriched in $\delta^{13}C$ (Fig. 2c and Supplementary Table 2). $\delta^{13}C$-SOC enrichment profiles like the one observed in Kahuzi-Biéga National Park are generally attributed to higher contributions of microbially derived and processed C with depth[27] and the Suess effect[28]. Together, these coupled DOC and SOC isotopic values suggest that deforested catchments export aged C from deeper soil horizons while forest-dominated catchments export modern terrestrial C leached from near the soil surface.

Changing DOM composition with land-use conversion

In addition to DOC age and source, the molecular composition of DOM was strongly controlled by the extent of deforestation in a catchment. Using ultrahigh-resolution mass spectrometry (Fourier-transform ion cyclotron resonance mass spectrometry (FT-ICR MS), see Methods) of solid-phase extractable DOM, we detected 17,560 distinct molecular formulae across all catchments, with an average of 10,493 formulae present in each sample (Supplementary Table 3). The average mass and aromaticity index—a measure of molecular stability with regard to biological degradation[29]—of DOM were found to be negatively correlated with deforestation extent (Supplementary Fig. 1a,b, respectively). In other words, DOM mobilized from deforested catchments was on average smaller and less aromatic in character than DOM exported from forested catchments, suggesting that it is vulnerable to microbial degradation. The chemodiversity of DOM, defined as the presence and proportion of other elements besides C and H, such as oxygen (O), nitrogen (N) and sulfur (S), is another important indicator of DOM source and quality[30]. Past studies have shown that anthropogenically impacted river catchments export DOM with greater relative abundances of N- and S-containing formulae[30,31]. On average, DOM from deforested catchments in this study exhibited higher fractions of N- and S-containing formulae (CHON and CHOS, respectively) relative to pristine catchments (Supplementary Fig. 2 and Supplementary Table 3).

Furthermore, the fraction of a sample's total relative abundance (signal magnitude), comprised of formulae classified as peptide-like, polyphenolic, unsaturated phenolic low-O/C, sugar-like and condensed aromatic (see Supplementary methods), were all found to be significantly correlated with deforestation extent. The fraction of total relative abundance from peptide-like and unsaturated phenolic low-O/C molecules increased with deforestation extent (Supplementary Fig. 1c,d), while the fraction from polyphenolic, condensed aromatic and sugar-like molecules decreased (Supplementary Fig. 1e,f,g and Supplementary Table 3). The fraction of total relative abundance from aliphatics and unsaturated high-O/C phenolics did not significantly correlate with deforestation extent (Supplementary Fig. 1h,i and Supplementary Table 3). These compound class results show that DOM sourced from deforested soils is highly reduced and more likely to contain N compared with DOM sourced from pristine, forested catchments.

To delve beyond the broad compound classes and assess how the relative abundances of individual molecular formulae correlated with deforestation extent and other environmental variables, we performed Spearman's rank correlations for each formula present in more than 50% of all samples (to include formulae sourced uniquely from forested or deforested end-members). FT-ICR MS detected

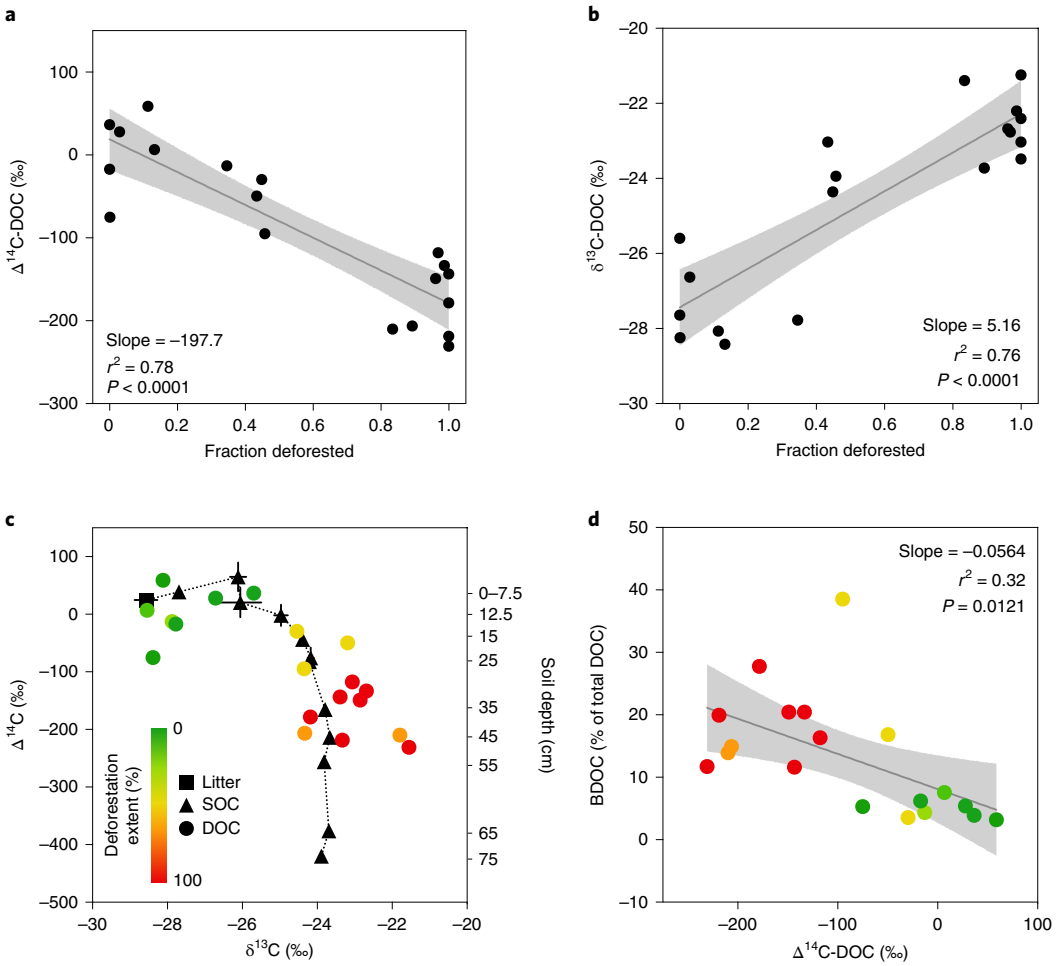

Fig. 2 | Isotopic indicators of stream DOC age, sources and biolability. a,**b**, Least-squares regressions between the fraction of deforestation and Δ^{14}C-DOC ($y=-197.7x+19.0$) (**a**) and fraction of deforestation and δ^{13}C-DOC ($y=5.16x-27.4$) (**b**) for all 19 catchments. **c**, Δ^{14}C versus δ^{13}C for streamwater DOC from 19 catchments (coloured circles) and SOC at different soil depths (given on the right *y*-axis) from a core taken in the pristine forest (black triangles with dotted line). Litter (black square) represents leaves and detritus from the forest floor above the core. Green-to-red colour bar indicates the fraction of deforestation of each catchment represented by the DOC point. Black error bars of the SOC data represent the standard deviation of values from the same depth of multiple cores, when available. **d**, Least-squares regression between Δ^{14}C-DOC and BDOC for all 19 catchments ($y=-0.056x+8.12$). The deforestation extent of each point is represented by the colour bar in panel **c**. Grey bands indicate 95% confidence intervals for **a**, **b** and **d**. 'Modern' radiocarbon value is +25‰ for **a**, **c** and **d**.

10,115 formulae present in at least half of all samples, 5,270 (52.1%) of which had relative abundances that were significantly correlated with deforestation extent (average absolute-value Spearman's rank correlation coefficient, $\rho_s=0.64$; $P<0.05$). Formulae with similar ρ_s values and signs were found to be grouped into two distinct assemblages in van Krevelen space (Fig. 3a). Formulae with relative intensities that were positively correlated with deforestation extent ($\rho_s>0$) generally had high H/C and moderately low O/C ratios, whereas negatively correlated formulae ($\rho_s<0$) displayed the opposite trend with the exception of one small cluster of high H/C (~1.25) and low O/C (~0.3) formulae commonly ascribed to lipid-like compounds[32]. Nearly identical groups of formulae were found to be correlated with δ^{13}C-DOC (Fig. 3b) and biolabile DOC (BDOC; Fig. 3c). When formulae relative abundances were correlated with forest extent, Δ^{14}C-DOC and DOC concentration, the same two assemblages emerged with inverse coefficient signs (Fig. 3d–f).

The two compositional assemblages revealed by FT-ICR MS correspond well to modern forest vegetation and aged SOC as end-member sources for exported DOM. Vascular plant-derived DOM is generally low H/C, high O/C and aromatic in nature[33–35], similar to the assemblage of formulae positively correlated with forest extent (Fig. 3d). Aged SOC, however, displays a composition similar to microbial biomass, with high H/C ratios, high N content from proteins and low aromaticity[35–38]. Our FT-ICR MS results show that formulae with this 'microbial' signature are strongly positively correlated with deforestation extent (Fig. 3a) and negatively correlated with Δ^{14}C-DOC (Fig. 3e). Overall, these patterns correspond well with our isotopic results, as well as with recent research on the controls of DOM composition that link landscape disturbance to the export of aged, aliphatic, protein-like and microbial DOM[18,30,38,39]. Consequently, we believe that the observed clear delineation of DOM composition concurrent with deforestation extent highlights the potential for future studies to fingerprint as well as develop unique molecular tracers for land-use change.

High biolability of aged DOC

To understand how deforestation controls the fate of DOM mobilized from disturbed soils, we conducted 28 d biolability incubations of streamwater DOC inoculated with ambient microorganisms. We found the fraction of BDOC (%) increased significantly with

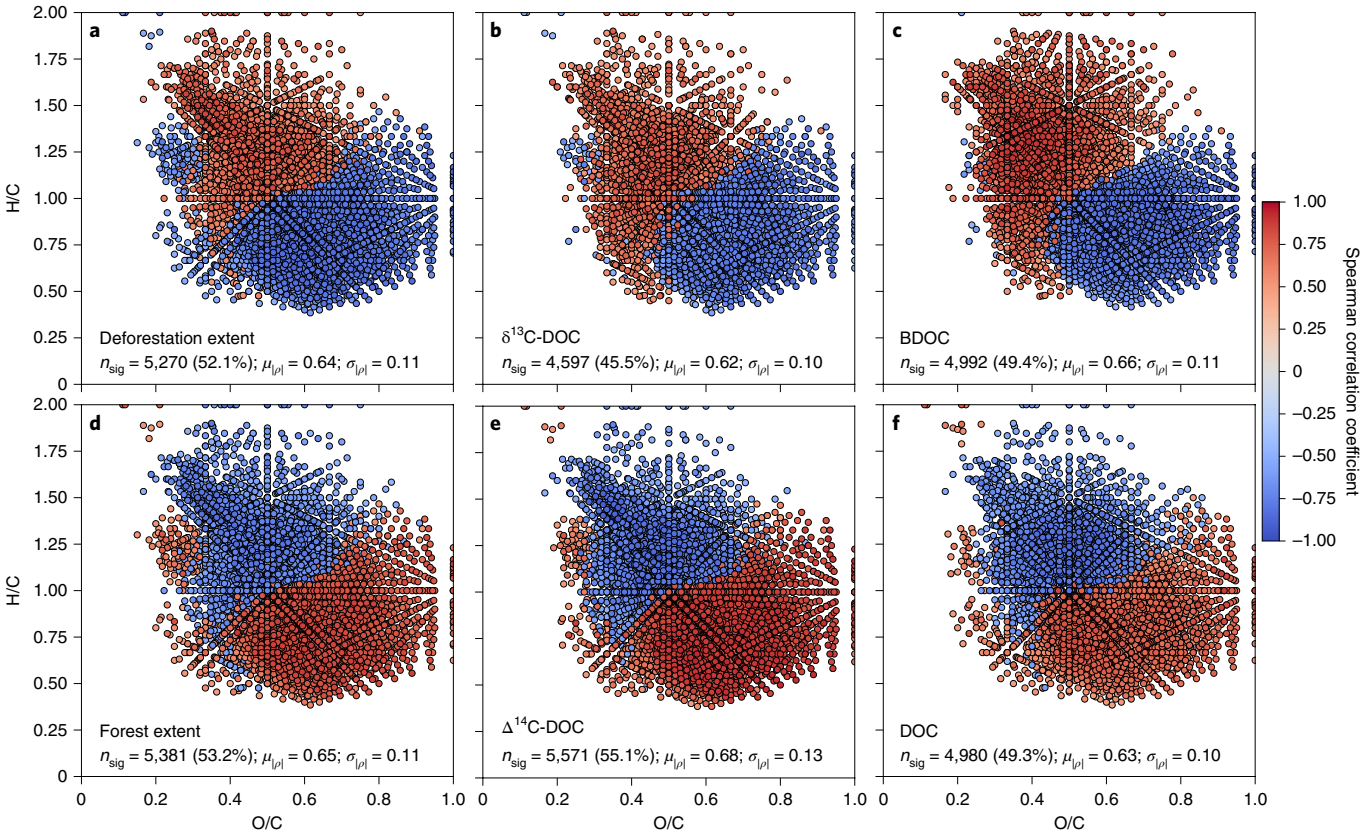

Fig. 3 | Van Krevelen diagrams of molecular formulae as a function of six environmental variables. a–f, Spearman-rank correlations of relative intensities for each molecular formula and deforestation extent (**a**), δ^{13}C-DOC (**b**), BDOC (**c**), forest extent (**d**), Δ^{14}C-DOC (**e**) and DOC concentration (**f**). Colours represent the correlation coefficient (ρ_s) between the relative intensity of each molecular formula and the given environmental variable. Red formulae (positive ρ_s) are more abundant in samples where the given environmental variable is high while blue formulae (negative ρ_s) are more abundant when the variable is low. The n_{sig} is the number of significantly correlated formulae for each variable. Proportion of common formulae comprised by n_{sig} are shown in parentheses. Also listed are the mean (μ) and standard deviation (σ) of the absolute value of $|\rho_s|$ for all formulae displayed in each panel.

deforestation extent (Supplementary Fig. 3a and Supplementary Table 1) and was negatively correlated with Δ^{14}C-DOC (Fig. 2d and Supplementary Table 1). Our linear model predicts that 19 ± 3% of DOC was biodegraded and respired to CO_2 in completely deforested catchments, compared with only 6.1 ± 3.1% in the pristine forested catchments.

Our data indicate that aged DOC mobilized from disturbed soils is substantially more biolabile than recently fixed C sourced from forested catchments. The compositional differences outlined in the section above explain this observed difference in biolability; DOM found in deforested catchments with high H/C ratios (that is, energy rich), high abundance of N-containing formulae, and low aromaticity is known to be highly biolabile[40–42]. Indeed, our results show that the relative abundance of such formulae were positively correlated with BDOC (red points in Fig. 3c). Conversely, molecular formulae assigned as polyphenolics and condensed aromatics are often stable over the timescale of water transit within these catchments[43]. Formulae with these characteristics were negatively correlated with BDOC (blue points in Fig. 3c).

The high biolability of aged DOC derived from deforested and agriculturally impacted soils observed in this study adds support to the emerging understanding that DOM biolability is independent of age. Recent glacier and permafrost studies have challenged the paradigm that old DOC is refractory by demonstrating high biolability of aged C[20,43–45]. Taken together with the results here, this suggests biolability is driven by the physicochemical conditions under which OM is formed and preserved and not solely by time since photosynthesis[46–48]. In deeper soil horizons of the forested catchments in the Congo Basin, SOC has most likely been stabilized via organo-mineral complexation and/or physical disconnection from decomposers and enzymes. Subsequent deforestation and removal of surface soils then alters the physicochemical conditions of these deeper layers, resulting in the breakdown of organo-mineral complexes and the loss of physical protection, ultimately leading to the release and mobilization of aged but chemically biolabile OM to aquatic ecosystems.

The observed high biolability of DOC in deforested catchments may lead to higher rates of respiration of OC relative to forest catchments. In both forested and deforested catchments, dissolved oxygen undersaturation indicates that respiration dominates over photosynthesis (Supplementary Fig. 4b and Supplementary Table 1). In the deforested streams, however, the byproduct of respiration, dissolved CO_2, was about 900 ppm higher than in forested streams (Supplementary Fig. 4c and Supplementary Table 1). Moveover, streamwater temperatures were about 5 °C higher (Supplementary Fig. 4d and Supplementary Table 1), potentially facilitating faster rates of bacterial respiration[49]. Similar agricultural land use-driven warming of stream ecosystems has been observed in the Amazon Basin and was attributed to the loss of both riparian shade and forest transpiration[50]. Collectively, these BDOC, dissolved oxygen, CO_2 and temperature results suggest that deforested catchments mineralize a greater proportion of DOC than forested catchments. Hence, streams draining deforested catchments are likely to outgas both more and older C as CO_2.

Table 1 | Predicted area-weighted annual fluxes of water, DOC and BDOC from pristine forest and deforested end-member catchments

	Water ($m\,yr^{-1}$)	DOC ($kg\,km^{-2}\,yr^{-1}$)	BDOC ($kg\,km^{-2}\,yr^{-1}$)
Pristine forest	0.41	1,597 ± 262	78 ± 26
Deforested	0.59	674 ± 228	126 ± 22
Change (%)	+44%	−56%	+66% (NS)

Error ranges are the standard error of the predicted end-member values from the linear regression. Change (%) is the relative difference of the deforested fluxes compared with the pristine fluxes. Note that the percentage change for BDOC is not statistically significant (NS).

Impact of land-use change on carbon yields

Ultimately, the absolute impact of the loss of pristine tropical forests on the mobilization of DOM depends on the difference in size and quality of DOM fluxes between deforested and forested catchments. Across our 19 catchments, DOC concentration was negatively related to deforestation extent (Supplementary Fig. 4d). To estimate water yields for the forested and deforested end-members, we used a regionally calibrated precipitation model (see Methods) that incorporates infiltration and plant evapotranspiration. Owing to the higher rates of evapotranspiration in the pristine forest catchments, our model predicts they export 0.41 $m\,yr^{-1}$ of water while deforested catchments export 0.59 $m\,yr^{-1}$ (Table 1).

Given these water yields and the DOC concentrations measured during the wet season (when >90% of annual discharge occurs; Supplementary Fig. 5a), we estimate that pristine forests yield ~1,597 $kg\,km^{-2}\,yr^{-1}$ of DOC, more than double the yield of deforested catchments (~708 $kg\,km^{-2}\,yr^{-1}$; Table 1 and Supplementary Fig. 5b). We attribute this to the simple fact that in general, above- and below-ground productivity in central African forests is significantly higher than croplands, and therefore more OC is available to be mobilized into streams[2,51]. Importantly, despite the significantly higher bulk DOC yields from forests, they do not export more BDOC than deforested catchments (Table 1 and Supplementary Fig. 5c). This is due to the higher BDOC concentrations observed in the deforested catchments. These estimated yields, together with the higher CO_2 concentrations and temperatures observed in deforested catchments, suggest that the loss of forests and conversion to agriculture increases both the rate of aquatic C respiration and the proportion of mineralized SOC available for outgassing from streams.

Using the above DOC yields, we tested whether the observed DOC isotopic and DOM compositional trends with deforestation could have resulted simply from loss of modern forest vegetation that masked background inputs of old OC in the forest sites. An isotopic mass-balance model was used to derive the hypothetical $\Delta^{14}C$ value of modern DOC (DOC_{young}) needed to mask old DOC inputs and produce a composite forest signature (DOC_{forest}) of 19.0‰ (Fig. 2a). The model yielded a super-modern DOC_{young} value of 177‰, which is significantly higher than recent leaf litter (~25–30‰), the most enriched SOC in Kahuzi-Biéga (65.2‰, 2.5 cm depth; Supplementary Table 2) and sites from throughout the Congo Basin (50.4–93.7‰)[52]. This suggests that forests could not realistically mask the equivalent export of old DOC as from deforested catchments (Supplementary methods). Moreover, DOM from deforested catchments exhibited unique molecular formulae relative to forested catchments (Supplementary Fig. 6). These formulae were predominantly heteroatomic and nearly identical to the assemblage correlated with older DOC (blue points in Fig. 3e). Simply put, these formulae do not exist in the forested catchments and thus represent an additional and likely older source of DOC to deforested catchments.

Reversing the forest carbon sink

Our results suggest that deforestation and the subsequent disturbance from agricultural land use reverses microbially mediated C stabilization in deep (forest) soils and increases the downstream export of biolabile and aged OC derived from deeper soil horizons. Deforestation therefore interrupts these natural C-cycling pathways and hastens the mobilization, biomineralization and transfer of old soil C to the atmosphere via the aquatic pathway.

Our coupled isotope results of catchment DOC and pristine forest SOC suggest that SOC originating from at least 0.5 m is being mobilized to rivers in deforested catchments (Fig. 2c). This half-metre soil denudation depth may also be conservative, as the higher rates of biomineralization of aged OC from deeper soils may preferentially remove old C and result in a more enriched $\Delta^{14}C$-DOC signature (shifting the apparent bulk signature towards a younger, shallower source). Regardless, this process signals a rapid loss of post-deforestation surface soils that have accumulated over hundreds to thousands of years of weathering.

The population of the DRC has grown from 15 million to 81 million people since the end of the Belgian colonial era in 1960 and is projected to grow more than fourfold by 2100[53,54]. To prevent an exacerbation of the patterns observed in this study and reduce erosion, maintain soil fertility and retain previously stabilized C, the implementation of modified agricultural techniques based on soil conservation practices (for example, terracing, buffer strips, incorporation of organic residues and so on) will be required[55]. Ultimately, we suggest that the retention of old and biolabile SOC that is currently stabilized and isolated from the modern C cycle is dependent on the conservation of forests and the related deceleration of land-use conversion in eastern Congo.

Online content

Any methods, additional references, Nature Research reporting summaries, source data, statements of code and data availability and associated accession codes are available at https://doi.org/10.1038/s41561-019-0384-9.

Received: 12 July 2018; Accepted: 10 May 2019;
Published online: 24 June 2019

References

1. Köchy, M., Hiederer, R. & Freibauer, A. Global distribution of soil organic carbon—Part 1: masses and frequency distributions of SOC stocks for the tropics, permafrost regions, wetlands, and the world. *Soil* **1**, 351–365 (2015).
2. Don, A., Schumacher, J. & Freibauer, A. Impact of tropical land-use change on soil organic carbon stocks—a meta-analysis. *Glob. Change Biol.* **17**, 1658–1670 (2011).
3. Schlesinger, W. H. & Andrews, J. A. Soil respiration and the global carbon cycle. *Biogeochemistry* **48**, 7–20 (2000).
4. Houghton, R. A. The annual net flux of carbon to the atmosphere from changes in land use 1850–1990. *Tellus B Chem. Phys. Meteorol.* **51**, 298–313 (1999).
5. Guo, L. B. & Gifford, R. M. Soil carbon stocks and land use change: a meta analysis. *Glob. Change Biol.* **8**, 345–360 (2002).
6. Stanley, E. H., Powers, S. M., Lottig, N. R., Buffam, I. & Crawford, J. T. Contemporary changes in dissolved organic carbon (DOC) in human-dominated rivers: is there a role for DOC management? *Freshw. Biol.* **57**, 26–42 (2012).
7. Schelker, J., Grabs, T., Bishop, K. & Laudon, H. Drivers of increased organic carbon concentrations in stream water following forest disturbance: separating effects of changes in flow pathways and soil warming. *J. Geophys. Res. Biogeosci.* **118**, 1814–1827 (2013).
8. Chow, A. T., Dahlgren, R. A. & Harrison, J. A. Watershed sources of disinfection byproduct precursors in the Sacramento and San Joaquin rivers, California. *Environ. Sci. Technol.* **41**, 7645–7652 (2007).
9. Chen, X. & Driscoll, C. T. Watershed land use controls on chemical inputs to Lake Ontario embayments. *J. Environ. Qual.* **38**, 2084–2095 (2009).
10. Meyer, J. L. & Tate, C. M. The effects of watershed disturbance on dissolved organic carbon dynamics of a stream. *Ecology* **64**, 33–44 (1983).
11. Cronan, C. S., Piampiano, J. T. & Patterson, H. H. Influence of land use and hydrology on exports of carbon and nitrogen in a Maine river basin. *J. Environ. Qual.* **28**, 953–961 (1999).

12. Moore, S. et al. Deep instability of deforested tropical peatlands revealed by fluvial organic carbon fluxes. *Nature* **493**, 660–663 (2013).
13. Rixen, T., Baum, A., Wit, F. & Samiaji, J. Carbon leaching from tropical peat soils and consequences for carbon balances. *Front. Earth Sci.* **4**, 563 (2016).
14. Butman, D. E., Wilson, H. F., Barnes, R. T., Xenopoulos, M. A. & Raymond, P. A. Increased mobilization of aged carbon to rivers by human disturbance. *Nat. Geosci.* **8**, 112–116 (2014).
15. Lu, Y. H. et al. Effects of land use on sources and ages of inorganic and organic carbon in temperate headwater streams. *Biogeochemistry* **119**, 275–292 (2014).
16. Raymond, P. A. & Bauer, J. E. Riverine export of aged terrestrial organic matter to the North Atlantic Ocean. *Nature* **409**, 497–500 (2001).
17. Mayorga, E. et al. Young organic matter as a source of carbon dioxide outgassing from Amazonian rivers. *Nature* **436**, 538–541 (2005).
18. Barnes, R. T., Butman, D. E., Wilson, H. F. & Raymond, P. A. Riverine export of aged carbon driven by flow path depth and residence time. *Environ. Sci. Technol.* **52**, 1028–1035 (2018).
19. Mann, P. J. et al. Utilization of ancient permafrost carbon in headwaters of Arctic fluvial networks. *Nat. Commun.* **6**, 7856 (2015).
20. Hood, E. et al. Glaciers as a source of ancient and labile organic matter to the marine environment. *Nature* **462**, 1044–1047 (2009).
21. Nachtergaele, F. et al. *Harmonized World Soil Database* Version 1.1 (ISRIC, 2009, accessed June 2018).
22. Dargie, G. C. et al. Age, extent and carbon storage of the central Congo Basin peatland complex. *Nature* **542**, 86–90 (2017).
23. Ickowitz, A., Slayback, D., Asanzi, P. & Nasi, R. *Agriculture and Deforestation in the Democratic Republic of the Congo: A Synthesis of the Current State of Knowledge* (CIFOR, 2015).
24. Hansen, M. C. et al. High-resolution global maps of 21st-century forest cover change. *Science* **342**, 850–853 (2013).
25. Potapov, P. V. et al. Quantifying forest cover loss in Democratic Republic of the Congo, 2000–2010, with Landsat ETM+data. *Remote Sens. Environ.* **122**, 106–116 (2012).
26. Kabonyi, C., Roche, E. & Gerrienne, P. Paléoenvironnements et paléoclimats durant le Pléistocène supérieur et l'Holocène sur la dorsale occidentale du Kivu en République Démocratique du Congo. *Eur. Sci. J.* **11**, 38–63 (2015).
27. Boström, B., Comstedt, D. & Ekblad, A. Isotope fractionation and ^{13}C enrichment in soil profiles during the decomposition of soil organic matter. *Oecologia* **153**, 89–98 (2007).
28. Rumpel, C. & Kögel-Knabner, I. Deep soil organic matter—a key but poorly understood component of terrestrial C cycle. *Plant Soil* **338**, 143–158 (2011).
29. Koch, B. P. & Dittmar, T. From mass to structure: an aromaticity index for high-resolution mass data of natural organic matter. *Rapid Commun. Mass Spectrom.* **20**, 926–932 (2006).
30. Wagner, S. et al. Linking the molecular signature of heteroatomic dissolved organic matter to watershed characteristics in world rivers. *Environ. Sci. Technol.* **49**, 13798–13806 (2015).
31. Riedel, T. et al. Molecular signatures of biogeochemical transformations in dissolved organic matter from ten world rivers. *Front. Earth Sci.* **4**, G01004 (2016).
32. D'Andrilli, J., Cooper, W. T., Foreman, C. M. & Marshall, A. G. An ultrahigh-resolution mass spectrometry index to estimate natural organic matter lability. *Rapid Commun. Mass Spectrom.* **29**, 2385–2401 (2015).
33. Stubbins, A. et al. Illuminated darkness: molecular signatures of Congo River dissolved organic matter and its photochemical alteration as revealed by ultrahigh precision mass spectrometry. *Limnol. Oceanogr.* **55**, 1467–1477 (2010).
34. Spencer, R. G. M. et al. Utilizing chromophoric dissolved organic matter measurements to derive export and reactivity of dissolved organic carbon exported to the Arctic Ocean: a case study of the Yukon River, Alaska. *Geophys. Res. Lett.* **36**, L06401 (2009).
35. Kellerman, A. M. et al. Unifying concepts linking dissolved organic matter composition to persistence in aquatic ecosystems. *Environ. Sci. Technol.* **52**, 2538–2548 (2018).
36. Kaiser, K. & Kalbitz, K. Cycling downwards-dissolved organic matter in soils. *Soil Biol. Biochem.* **52**, 29–32 (2012).
37. Kögel-Knabner, I., Totsche, K. U. & Raber, B. Desorption of polycyclic aromatic hydrocarbons from soil in the presence of dissolved organic matter: effect of solution composition and aging. *J. Environ. Qual.* **29**, 906–916 (2000).
38. Wilson, H. F. & Xenopoulos, M. A. Effects of agricultural land use on the composition of fluvial dissolved organic matter. *Nat. Geosci.* **2**, 37–41 (2008).
39. Creed, I. F. et al. Global change-driven effects on dissolved organic matter composition: implications for food webs of northern lakes. *Glob. Change Biol.* **24**, 3692–3714 (2018).
40. Berggren, M., Laudon, H., Haei, M., Ström, L. & Jansson, M. Efficient aquatic bacterial metabolism of dissolved low-molecular-weight compounds from terrestrial sources. *ISME J.* **4**, 408–416 (2010).
41. van Hees, P. A. W., Jones, D. L., Finlay, R., Godbold, D. L. & Lundström, U. S. The carbon we do not see—the impact of low molecular weight compounds on carbon dynamics and respiration in forest soils: a review. *Soil Biol. Biochem.* **37**, 1–13 (2005).
42. Kalbitz, K. et al. Changes in properties of soil-derived dissolved organic matter induced by biodegradation. *Soil Biol. Biochem.* **35**, 1129–1142 (2003).
43. Spencer, R. G. M. et al. Detecting the signature of permafrost thaw in Arctic rivers. *Geophys. Res. Lett.* **42**, 2830–2835 (2015).
44. Singer, G. A. et al. Biogeochemically diverse organic matter in Alpine glaciers and its downstream fate. *Nat. Geosci.* **5**, 710–714 (2012).
45. Spencer, R. G. M. et al. Source and biolability of ancient dissolved organic matter in glacier and lake ecosystems on the Tibetan Plateau. *Geochim. Cosmochim. Acta* **142**, 64–74 (2014).
46. Schmidt, M. W. I. et al. Persistence of soil organic matter as an ecosystem property. *Nature* **478**, 49–56 (2011).
47. Kögel-Knabner, I. The macromolecular organic composition of plant and microbial residues as inputs to soil organic matter. *Soil Biol. Biochem.* **34**, 139–162 (2002).
48. Denef, K., Planet, A. F. & Six, J. in *Soil Carbon Dynamics: An Integrated Methodology* (eds Kutsch, W. L. et al.) 91–126 (Cambridge Univ. Press, 2009).
49. Demars, B. O. L. et al. Temperature and the metabolic balance of streams. *Freshw. Biol.* **56**, 1106–1121 (2011).
50. Macedo, M. N. et al. Land-use-driven stream warming in southeastern Amazonia. *Phil. Trans. R. Soc. Lond. B* **368**, 20120153 (2013).
51. Baccini, A., Laporte, N., Goetz, S. J., Sun, M. & Dong, H. A first map of tropical Africa's above-ground biomass derived from satellite imagery. *Environ. Res. Lett.* **3**, 045011 (2008).
52. Spencer, R. G. M. et al. An initial investigation into the organic matter biogeochemistry of the Congo River. *Geochim. Cosmochim. Acta* **84**, 614–627 (2012).
53. Gerland, P. et al. World population stabilization unlikely this century. *Science* **346**, 234–237 (2014).
54. *World Population Prospects 2017* (United Nations, 2017); https://esa.un.org/unpd/wpp/
55. Govers, G., Merckx, R., Van Oost, K. & van Wesemael, B. *Managing Soil Organic Carbon for Global Benefits: A Stap Technical Report* (Global Environmental Facility, 2013).

Acknowledgements

We thank our network of collaborators at the International Institute of Tropical Agriculture and the Université Catholique de Bukavu in DR Congo for their local expertise and logistical assistance. Funding for this research was provided by the Winchester Fund at Florida State University. This work was partially supported by National Science Foundation grants OCE 1464396 to R.G.M.S., and DMR-1157490 and DMR-1644779 to the National High Magnetic Field Laboratory. K.V.O. received funding from FNRS. A.M.H. and S.E.T. received funding from the European Research Council under the European Union's Horizon 2020 research and innovation programme (grant agreement no. 695101 (14 Constraint)).

Author contributions

T.W.D., R.G.M.S., J.S., and K.V.O. conceived the study. T.W.D., M.Barthel and M.Bauters carried out the fieldwork and sample collection. T.W.D., M.Barthel, M.Bauters, A.M.H. and D.C.P. performed sample analyses. T.W.D., K.V.O. and M.Bauters performed geospatial analyses. L.C.N. provided logistical support in DR Congo. T.W.D. wrote the manuscript with significant contributions from M.Bauters, A.M.H., J.S., P.B., S.E.T. and R.G.M.S.

Competing interests

The authors declare no competing interests.

Additional information

Supplementary information is available for this paper at https://doi.org/10.1038/s41561-019-0384-9.

Reprints and permissions information is available at www.nature.com/reprints.

Correspondence and requests for materials should be addressed to T.W.D.

Publisher's note: Springer Nature remains neutral with regard to jurisdictional claims in published maps and institutional affiliations.

Methods

Site description and deforestation extent classification. The 19 catchments sampled for this study lie on the western side of Lake Kivu to the north and south of the city of Bukavu, DRC (Fig. 1). We selected the region near Bukavu for this study due to the proximity of contrasting agricultural land use and pristine forests. The pristine forest catchments, found almost exclusively within the protected Kahuzi-Biéga National Park boundaries, are dominated by a mixed, evergreen, broadleaf tree assemblage. Areas of deforested cropland are nearly treeless with a patchwork of small agricultural plots usually containing a mix of maize, beans, sorghum, banana, onion, cassava and unplanted bare soil. Catchment boundaries were delineated using the TauDEM terrain analysis tool[56] along with a 1 arc second (ca. 30 m) digital elevation model (DEM)[57] and the GPS locations of our sampling points. Catchments were then uploaded to Google Earth Engine and analysed for the fraction deforested using the Moderate Resolution Imaging Spectroradiometer (MODIS) 2013 Land Cover dataset (MCD12Q1)[58]. Because historically forests covered the entire Kivu region before widespread human settlement[26], all non-forested land cover was considered 'deforested' for the purpose of this study. As a result, deforested fractions were calculated as the fraction of the catchment containing no evergreen broadleaf forest or mixed forest, the only two forest classifications contained by the study catchments (MODIS classifications 2 and 5, respectively). Temporal changes in deforestation extent were assessed using historic European Space Agency Climate Change Initiative Land Cover data (http://maps.elie.ucl.ac.be/CCI/viewer/index.php) and found to be minimal over the past decade.

Sample collection and measurement. Water was collected from 19 streams near lake Kivu, DRC during the wet season in April 2017. The wet season was chosen because it comprises more than nine months of the year and represents nearly all of the annual water flux through streams (>90%). Streams were well mixed and varied in width from approximately 1 to 3 m. All samples were collected from the thalweg of the streams at approximately 15 cm depth below the water surface. Field measurements for dissolved oxygen, pH and temperature were taken with a pre-calibrated YSI ProDSS multimeter sonde. Dissolved CO_2 concentrations were measured with a pre-calibrated EOSense CO_2 Concentration probe (eosGP) that was allowed to equilibrate with the stream water for at least 45 min. All water samples were filtered in the field with pre-combusted (450 °C, >5 h) 0.7 µm glass microfiber filters into pre-washed and 1 N HCl acid-leached polycarbonate bottles. Water samples were preserved via acidification to a pH of 2 with 12 N HPLC-grade HCl the same day of sampling. The acidified water samples were analysed for DOC concentrations via high-temperature catalytic oxidation on a Shimadzu TOC-L CPH total organic carbon analyser at Florida State University using established methodology[59]. Soil samples were taken from three 22.5 cm and one 75 cm soil cores extracted from the pristine forest in Kahuzi-Biéga National Park (2.31314° S, 28.75471° E). In addition, plant litter samples were taken from the forest floor around the soil cores. From each depth, approximately 100 g of soil were collected and air dried for 48 h before being sealed and transported to the laboratory at ETH Zurich where soils were dried in a drying oven (50 °C) and subsequently ball milled.

Carbon isotope analyses. For each site, 500 ml of filtered and acidified water were sent to the National Ocean Sciences Accelerator Mass Spectrometry (http://www.whoi.edu/nosams/home) laboratory in Woods Hole for analysis of δ^{13}C-DOC and Δ^{14}C-DOC. Prepared soil and litter samples were analysed at ETH Zurich for δ^{13}C-SOC using an elemental analyser (Flash EA, Thermo Fisher Scientific) coupled to a Delta^{plus}XP Isotope Ratio Mass Spectrometer via a six-port valve and a ConFlo III interface (both Finnigan MAT)[60,61]. Soil subsamples were sent to the Max Planck Institute for Biogeochemistry for Δ^{14}C-SOC analysis. Soil samples were combusted and graphitized following Steinhof et al.[62] before analysis on a MICADAS ^{14}C AMS system (Ionplus AG). Leaf litter samples were assigned a modern radiocarbon value (+25‰) based on the 2016–2017 atmospheric CO_2 radiocarbon content[63]. All resulting ^{13}C/^{12}C ratios are reported in δ^{13}C notation relative to Vienna Pee Dee Belemnite and radiocarbon ratios are reported in Δ^{14}C notation following ref. [64].

FT-ICR MS analysis. DOM in streamwater samples was isolated for FT-ICR MS analysis via solid-phase extraction with 100 mg Bond Elut (Agilent Technologies) styrene-divinylbenzene copolymer (PPL) columns. Depending on a sample's DOC concentration, the volume used for extraction was adjusted such that 50 µg of C was eluted with 1 ml of HPLC-grade methanol into a pre-combusted glass vial. The molecular composition of PPL-extracted DOM was determined using the 21-Tesla FT-ICR MS at the National High Magnetic Field Laboratory at Florida State University[65,66]. Negative ions were generated by injecting the extracted sample into the mass spectrometer via negative electrospray ionization at a flow rate of 500 nl min^{-1}. Mass spectra were generated as the sum of 100 individual spectra scans for each sample. See Supplementary Text for formula assignment methods.

Biolability incubation experiments. Bioincubations of DOC (BDOC) were performed using established methods[59]. Briefly, bioincubations were initiated by injecting 30 ml of 0.7 µm filtered stream water into six pre-evacuated and pre-weighed 60 ml borosilicate serum vials. Three serum vials were immediately acidified to a pH of 2 (t0) using 12 N HPLC-grade HCl and the remaining three vials were allowed to incubate in the dark at room temperature for 28 d (t28) before acidification to a pH of 2. Each serum vial was then weighed, re-pressurized with helium and allowed to equilibrate for 1 d before the concentration of CO_2 in the headspace was analysed on a gas chromatograph at Florida State University. Using Henry's law, CO_2 concentrations (equivalent to total dissolved inorganic carbon concentrations at pH of 2) were determined by the volume of water in each serum vial and the concentration of CO_2 in the headspace. The difference in dissolved inorganic carbon concentrations between the averaged t28 and t0 timepoints was attributed to CO_2 produced by microbial respiration during the 28 d incubation. BDOC percentages were calculated by the ratio of C as CO_2 produced to the initial (t0) DOC concentration[59].

Water and DOC yield estimates. Area-weighted annual water yields were determined for the pristine forested and deforested end-members using the US Army Corps of Engineers Hydrologic Engineering Center's Hydrologic Modeling System (http://www.hec.usace.army.mil/software/hec-hms/) paired with soil infiltration, vegetation transpiration and geomorphologic constraints for the Lake Kivu region. The model was calibrated with hourly precipitation and runoff data sourced from the Goma Volcanic Observatory in Goma, DRC on the north side of Lake Kivu. Sampling point GPS-located Tropical Rainfall Measuring Mission (https://pmm.nasa.gov/TRMM) precipitation data extrapolated over the total catchment area were used to estimate total annual precipitation ($m^3 yr^{-1}$) for each catchment. End-member-weighted water yields (proportion of precipitation as runoff, mm yr^{-1}) were then assigned to each catchment by deforestation extent. Total annual water yields for each catchment were then calculated by multiplying the modelled water yields by the total catchment area. Approximate annual DOC and BDOC yields were then calculated by multiplying the catchment-specific wet-season DOC and BDOC concentrations by the modelled annual water yields.

Statistical analyses. All least-squares regression analyses, including the determination of 95% confidence intervals, were performed with Graphpad Prism 6.0 software. Standard errors of predicted values were calculated using the 'Statsmodels' python package[67]. FT-ICR MS data analysis for compound class statistics, heteroatomic content and Spearman's rank correlations were performed with the 'fouriertransform' Python package[68].

Data availability

The authors declare that all data supporting the findings of this study other than non-categorized FT-ICR MS data are available within the paper and its supplementary information files. Non-categorized FT-ICR MS formulae data are available from the corresponding author upon request.

References

56. Tarboton, D. *TauDEM* Version 5 (accessed 15 February 2018); http://hydrology.usu.edu/taudem/taudem5/
57. *NASA Shuttle Radar Topography Mission Global 1 Arc Second* (NASA LP DAAC, 2013).
58. Friedl, M. A. et al. MODIS Collection 5 global land cover: algorithm refinements and characterization of new datasets. *Remote Sens. Environ.* **114**, 168–182 (2010).
59. Drake, T. W. et al. The ephemeral signature of permafrost carbon in an arctic fluvial network. *J. Geophys. Res. Biogeosci.* **123**, 1475–1485 (2018).
60. Werner, R. A., Bruch, B. A. & Brand, W. A. ConFlo III-an interface for high precision δ^{13}C and δ^{15}N analysis with an extended dynamic range. *Rapid Commun. Mass Spectrom.* **13**, 1237–1241 (1999).
61. Brooks, P. D., Geilmann, H., Werner, R. A. & Brand, W. A. Improved precision of coupled δ^{13}C and δ^{15}N measurements from single samples using an elemental analyzer/isotope ratio mass spectrometer combination with a post-column six-port valve and selective CO_2 trapping; improved halide robustness of the combustion reactor using CeO_2. *Rapid Commun. Mass Spectrom.* **17**, 1924–1926 (2003).
62. Steinhof, A., Altenburg, M. & Machts, H. Sample preparation at the Jena ^{14}C Laboratory. *Radiocarbon* **59**, 815–830 (2017).
63. Turnbull, J. C. et al. Sixty years of radiocarbon dioxide measurements at Wellington, New Zealand: 1954–2014. *Atmos. Chem. Phys.* **17**, 14771–14784 (2017).
64. Stuiver, M. & Polach, H. A. Discussion: reporting of ^{14}C data. *Radiocarbon* **19**, 355–363 (1977).
65. Smith, D. F., Podgorski, D. C., Rodgers, R. P., Blakney, G. T. & Hendrickson, C. L. 21 Tesla FT-ICR mass spectrometer for ultrahigh-resolution analysis of complex organic mixtures. *Anal. Chem.* **90**, 2041–2047 (2018).
66. Hendrickson, C. L. et al. 21 Tesla Fourier transform ion cyclotron resonance mass spectrometer: a national resource for ultrahigh resolution mass analysis. *J. Am. Soc. Mass Spectrom.* **26**, 1626–1632 (2015).
67. Seabold, S. & Perktold, J. Statsmodels: econometric and statistical modeling with python. In *Proc. 9th Python in Science Conference* 57–61 (SciPy Society, 2010).
68. Hemingway, J. D. fouriertransform: open-source tools for FT-ICR MS data analysis. *GitHub* https://github.com/FluvialSeds/fouriertransform (2017).